Using Superimposed ASK Label in a 10-Gb/s Multihop All-Optical Label Swapping System

Yu-Min Lin, Maria C. Yuang, San-Liang Lee, *Member, IEEE*, and Winston I. Way, *Fellow, IEEE, Fellow, OSA*

***Abstract*—A novel optical-label-swapping technique is proposed, experimentally verified, and theoretically analyzed in this paper. The technique superimposes a low-speed amplitude-shift-keying (ASK) label on top of a high-speed dc-balanced-line-coded ASK payload. A multihop long-distance transmission experiment using a recirculating loop has been successfully demonstrated, and an experimental record is set when compared with other optical-label-swapping techniques.**

***Index Terms*—Amplitude-shift-keying (ASK) labels, multihop transmission, optical label swapping, optical packet switching.**

I. Introduction

DENSE-WAVELENGTH-DIVISION-MULTIPLEXING (DWDM) transmission and generalized multiprotocol label switching (GMPLS) [1] are considered the key enabling technologies for the next-generation optical Internet backbone. In a GMPLS-based optical switch/router, the low-speed label associated with a high-speed payload is extracted, processed, and replaced at every intermediate network-switching node. Meanwhile, the high-speed payload is optically switched (controlled by the electrically processed label) to an appropriate output fiber as an entirely untouched entity. Therefore, a GMPLS-based optical switch/router is transparent to various payload data rates (10 Gb/s, 40 Gb/s, etc.) and formats (SONET, Gigabit, etc.), and could use economically realizable processors for the low-speed labels (e.g., a Fast Ethernet).

Many optical-label-swapping techniques have been proposed; among those, the time-domain-multiplexing technique [2] requires extremely precise control timing and alignment. The subcarrier-multiplexed labeling technique [3]–[5] requires an extra bandwidth beyond traditional baseband payload and requires stringent wavelength accuracy and stability if a fixed optical notch filter (e.g., a fiber Bragg grating) is used to erase the old label [3]. The orthogonal modulation technique, including amplitude shift keying (ASK)/frequency shift keying (FSK) [6] and ASK/differential phase shift keying (DPSK) [7], [8], exhibits severe transmission system penalty due to its inherently low extinction ratio of high-speed payload signal [9].

Manuscript received July 29, 2003; revised October 23, 2003. This work was supported in part by the MOE program of Excellence Research, Taiwan, R.O.C., under Contract 89-E-FA04-1-4 and in part by Computer & Communications Research Laboratories, Industrial Technology Research Institute (ITRI), Taiwan, R.O.C., under Contract A321XS1J20.

Y.-M. Lin is with the Department of Communications Engineering, National Chiao-Tung University, Hsinchu 300, Taiwan, R.O.C.

M. C. Yuang is with the Department of Computer Science and Information Engineering, National Chiao-Tung University, Hsinchu 300, Taiwan, R.O.C.

S.-L. Lee is with the Department of Electronic Engineering, National Taiwan University of Science and Technology, Taipei 673, Taiwan, R.O.C.

W. I. Way is with the OpVista, Inc., Irvine, CA 92618 USA.

Digital Object Identifier 10.1109/JLT.2004.824356

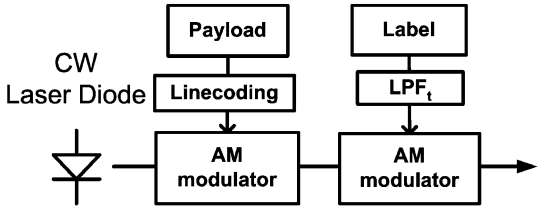

Fig. 1. Building blocks of an optical transmitter to generate a composite signal containing an ASK payload and an ASK label.

In this paper, we proposed a new modulation scheme that superimposes a low-speed ASK label on top of a high-speed dc-balanced line-coded ASK payload. An old ASK label is erased by modulating the combined payload and label signal with the inverse of the received ASK label. This ASK labeling technique requires only low-speed external modulators and low-speed optical receivers to perform the label swapping mechanism and does not require sophisticated optical components, such as Mach–Zehnder interferometer (MZI)–semiconductor optical amplifier (SOA) [7] to perform payload/label separation. Both analytical and experimental results are presented to prove the feasibility and scalability of this new scheme.

This paper is organized as follows. The operation principle of the proposed label-swapping technique is described in Section II. In Section III, an analysis on the system performance of the new scheme is presented. In Section IV, a transmission experiment using a recirculating loop is described. The correlation between the analytical and experimental results is described in Section V. In particular, the scalability and transmission performance of the new scheme are discussed. The conclusion of this paper is given in Section VI.

II. Operation Principle

As shown in Fig. 1, an optical transmitter is composed of two-stage intensity modulators: a continuous-wave (CW) light source is first modulated by a high-speed nonreturn-to-zero (NRZ) payload with a large modulation depth m_U and is then subsequently modulated by a low-speed NRZ label with a small modulation depth m_h. A dc-balanced line encoder was adopted to suppress the low frequency energy of the payload signal. We chose 8B/10B line code [10] because of its popularity in an Ethernet environment and because of its bandwidth efficiency (only 25% extra bandwidth is required). For a 10-Gb/s coded payload, the actual payload information

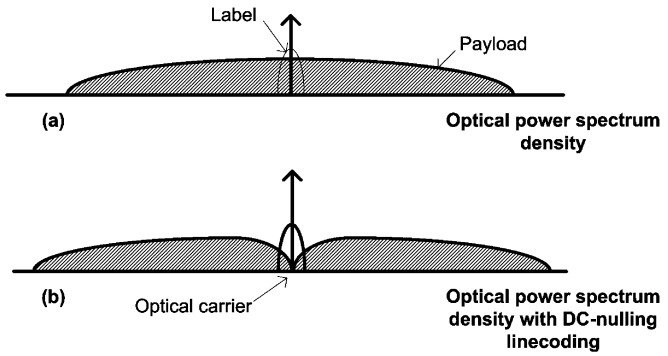

Fig. 2. (a) Optical power spectra of a high-speed payload (without linecoding) and a superimposed low-speed ASK label. (b) Optical power spectra of a high-speed payload (with line coding to remove low-frequency component) and a superimposed low-speed ASK label.

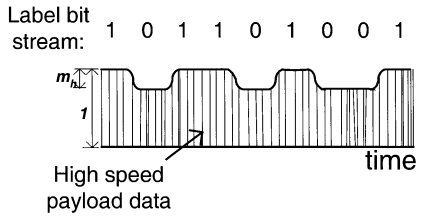

Fig. 3. Time-domain waveform of the composite signal which contains a high-speed payload data and a superimposed low-speed ASK label.

runs at 8 Gb/s. Figs. 2(a) and 3 show typical power spectra and a three-level optical intensity waveform with a small label peak modulation depth m_h. It can be seen in Fig. 2(a) that the label has a poor signal-to-interference ratio (SIR) when it is transmitted together with a payload with random sequence, and that is why a dc-balanced line encoder is needed.

The selection of a proper modulation depth for a label signal is important. This is because a label with a low modulation index could not sustain multihop long-distance transmission due to the payload interference and other transmission noise, while a label with a large modulation index could decrease the payload signal power (see Fig. 3), and causes higher residual noise due to nonideal label erasers.

The optical-label-swapping scheme implemented in each intermediate switching node is shown in Fig. 4, where we can see a label eraser module and a new label AM modulator. In the label eraser module, a portion of the input signal is detected through a passive optical tap and a photodiode. A low-pass filter $(\mathrm{LPF_r})$ at the receiver front end is used to remove most of the payload signal and out-of-band noise, whereas a limiting amplifier and a low-pass filter $(\mathrm{LPF_t})$ are used to provide a constant amplitude and reshape the received label waveform, respectively. The $\mathrm{LPF_t}$ in the switching node should have a frequency response as close to that of the transmitting end $\mathrm{LPF_t}$ (see Fig. 1) in order to inversely compensate the superimposed old label. Note that when the received label has a low-error-rate performance, it can be considered as an analog copy of original label signal. We use this reshaped label, called the *complementary signal*, to reverse-modulate the optical signal (via the AM modulator in Fig. 4 with a negative logic) with the same modulation depth m_h. In this way, most of the incoming (old) label can be removed. However, the intensity noise on the received label introduces timing jitter on the complementary signal when it passes through a limiting amplifier, and the jitter noise makes the label eraser imperfect. Note that a fiber delay line is placed before the AM modulator to minimize the deterministic phase error between the incoming and complementary signals.

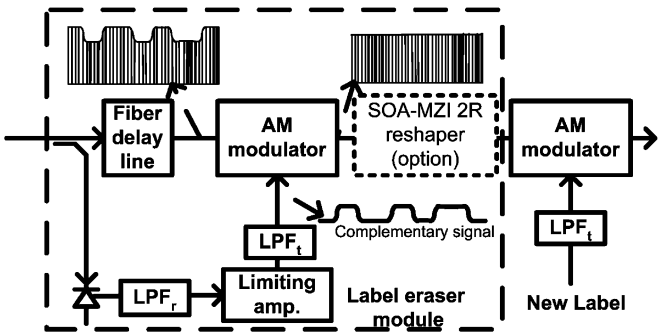

Fig. 4. Label-swapping apparatus, composed of a label eraser and a new label modulator.

If the number of hops along the optical path is large, and/or if the distance between switch/routers requires a cascade of many amplifiers, an additional all-optical reshaper [12] could be used to further suppress the residual intensity noise.

III. Performance Analysis

In this section, the transmission performance of a label and its associated payload is analyzed considering several dominant noise terms in the proposed scheme. We consider a linear optical system where optical fiber nonlinearity can be ignored and optical fiber dispersion is fully compensated. In Section III-A, we calculate the effect of payload interference on a label signal. In Section III-B, we calculate the effect of cascaded optical amplifier noise on a label signal in a multihop optical link. In Section III-C, the residual noise due to a nonideal label eraser, and its cumulative effect in a multihop transmission system, is calculated. The effects of receiver noise are briefly discussed in Section III-D. The overall Q-factor performances of a label and a payload are summarized in Sections III-E and F, respectively.

A. Effect of Payload-Induced Interference Noise on a Label Signal

Payload and label are baseband binary signal which can be expressed as

$$U(t) = \sum_i U_i p_U(t - iT_U) \tag{1}$$

for a payload, and

$$H(t) = \sum_i H_i p_h(t - iT_h) \tag{2}$$

for a label. In (1) and (2), H_i and $U_i \in \{1, 0\}$, and $p_U(t)$ and $p_h(t)$ are unit-amplitude pulses. At the transmitter end, the signal after two intensity modulators can be written as (3), shown at the bottom of the next page, where P_{peak} is the peak power level of the combined signal, and ω_c and θ are the frequency and phase of the optical carrier, respectively. The relationship between the peak and

the average power of the transmitted signal is given by $P_{\rm peak} = (P_{\rm avg})/((1-0.5m_U)(1-0.5m_h))$. The received photocurrent is given by $I(t) = R_{\rm ph}\kappa\langle E(t)\rangle^2$, where $R_{\rm ph}$ is the responsivity of the label receiver and κ is the coupling ratio of the optical tap. We define the average and peak label receiver input power as $P_h = \kappa P_{\rm avg}$ and $P_{h,\rm peak} = \kappa P_{\rm peak}$, respectively. The detected label photocurrent is given by $I_{h,1} = R_{\rm ph}P_{h,\rm peak}[(1-m_U)+m_U(1/2)]$ when $H(t) = 1$, and is given by $I_{h,0} = R_{\rm ph}P_{h,\rm peak}(1-m_h)[(1-m_U)+m_U(1/2)]$ when $H(t) = 0$. This is equivalent to saying that a slow label only sees the DC of a fast payload $U(t)$, i.e., $U(t)$ in (3) can be simply replaced by its DC value $1/2$ from the viewpoint of a label signal. Consequently, the peak-to-peak amplitude of a label signal is given by $R_{\rm ph}P_{h,\rm peak}[((1/2)m_U+(1-m_U))m_h]$. This received label signal amplitude will be used in the calculation of the Q factor.

The payload-induced interference noise power in a label is given by

$$\sigma^2_{\rm it,1} = (R_{\rm ph}P_{h,\rm peak}m_U)^2\int_{-\infty}^{\infty}|F_{\rm rh}(f)|^2S_U(f)\,df, \qquad H(t)=1$$
$$\sigma^2_{\rm it,0} = (R_{\rm ph}P_{h,\rm peak}(1-m_h)m_U)^2\int_{-\infty}^{\infty}|F_{\rm rh}(f)|^2S_U(f)\,df, \qquad H(t)=0 \quad (4)$$

where $F_{\rm rh}(f)$ is the Fourier transform of LPF_r at the label receiver front end (see Fig. 4). $S_U(f)$ is the power spectral density (PSD) of $U(t)$ which depends on both the line code, the pulse shape of the payload, and the length of the pseudorandom bit sequence (PRBS). However, note that when a line code is used, the length of the PRBS may not be a very important factor any more. In our case, the length of the payload's PRBS is not important because the maximum run length of the 8B/10B code is only 5 b.

In Fig. 5, the label SIRs, which are defined as $\mathrm{SIR} = ((I_{h,1}-I_{h,0}))/(\sigma_{\rm it,1}+\sigma_{\rm it,0})$ under different label bit rates are shown when the payload is 8B/10B coded (i.e., $S_U(f)$ in (4) is substituted with the power spectral density of an 8B/10B code [10], [11]). Based on Fig. 5, we choose a label data rate of 100 Mb/s and a modulation depth of 0.22 in our experiment in order to obtain an $\mathrm{SIR} > 20$ dB (20 dB is chosen to allow a > 4-dB margin from the theoretical 15.7-dB requirement to achieve a bit-error rate (BER) of 10^{-9}). Under this condition (a 100-Mb/s label versus an 8-Gb/s raw payload), a label of 8 B can be transmitted simultaneously with a composite packet payload of 640 B. This should generate acceptable latency in the packet assembly process at an edge router [13], [14].

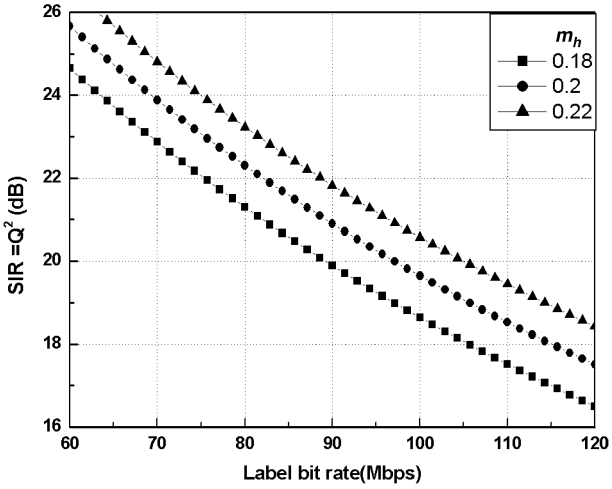

Fig. 5. Label SIR versus label bit rates at different m_h, when an 8B/10B-line-coded payload is used.

B. Cascaded Optical Amplifier Noise

The accumulated amplifier noise along a multihop optical path is calculated in this section. The system configuration with multiple optical amplifiers and switching nodes is shown in Fig. 6. Each switching node has two optical amplifiers, with the first one compensating transmission fiber loss and the second one compensating internal node loss due to multiple passive components [15]. $P_{\rm in}$ is the input power to the first-stage amplifier, and G_1 and G_2 are the gains of the first and second amplifier, respectively. L_1 and L_2 are the loss of passive components in a switching node. L_3 accounts for the loss due to dispersion compensation devices and fiber propagation loss in the next hop. In each switching node, all packets are received after the second amplifier, as shown in Fig. 6.

The received power at different nodes are kept constant as

$$P_{\rm out,(1)} = P_{\rm out,(k)} = P_{\rm in}G_1L_1G_2 \quad (5)$$

and the corresponding amplified spontaneous emission (ASE) noise power at the first hop is calculated as

$$P_{\rm ase,(1)} = [(P_{\rm ase1}L_1)G_2 + P_{\rm ase2}] \quad (6)$$

where $P_{\rm ase1} = 2n_{\rm sp}h\nu\Delta\nu_f(G_1-1)$ and $P_{\rm ase2} = 2n_{\rm sp}h\nu\Delta\nu_f(G_2-1)$ are the ASE noise power generated by the first and second amplifiers, respectively, where $n_{\rm sp}$ is the population inversion factor, $h\nu$ is the photon energy, and $\Delta\nu_f$ is the bandwidth of an optical bandpass filter. At the kth hop, we can calculate the ASE power as

$$P_{\rm ase,(k)} = k[(P_{\rm ase1}L_1)G_2 + P_{\rm ase2}]. \quad (7)$$

Finally, the dropped packet needs to go through a demultiplexer with a loss L. In our analytical model and experiment setup, L is

$$E(t) = \sqrt{P_{\rm peak}((1-m_U)+m_UU(t))}\sqrt{((1-m_h)+m_hH(t))}\exp(j\omega_ct+\theta)$$
$$= \sqrt{P_{\rm peak}[(1-m_U)(1-m_h)+(1-m_h)m_UU(t)+(m_h(1-m_U)+m_hm_UU(t))H(t)]}\exp(j\omega_ct+\theta) \quad (3)$$

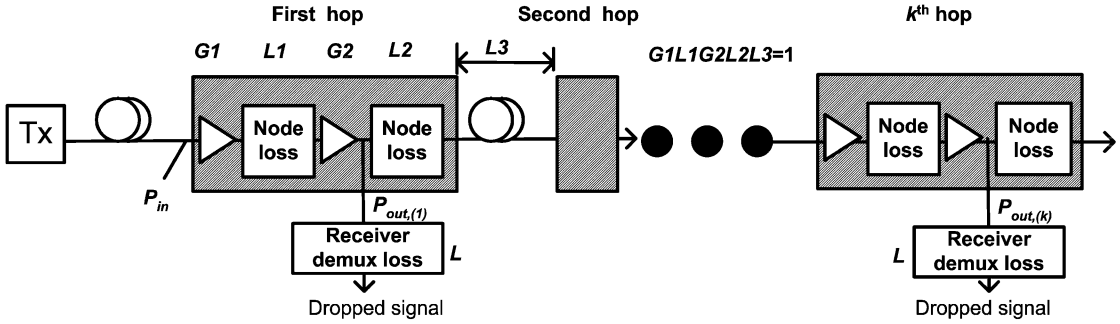

Fig. 6. Transmission system model for calculating the cascaded erbium-doped fiber amplifier (EDFA) noise in a multihop optical network.

adjusted to test receiver sensitivity. At the front end of the optical receiver at the kth hop, the average signal power and ASE power can be written as $P = LP_{\text{out},(k)}$ and $P_{\text{avgase},(k)} = LP_{\text{ase},(k)}$, respectively. The spontaneous–spontaneous and signal–spontaneous beat noise power are given by [16], [17]

$$\sigma^2_{\text{sp}-\text{sp},(k)} = (RP_{\text{avg,ase},(k)})^2(2 - B/\Delta v_f)(B/\Delta v_f) \quad (8)$$

$$\sigma^2_{\text{sig}-\text{sp},(k)} = 2RPRP_{\text{avg,ase},(k)} \quad (9)$$

where $B = B_{hr}$ and $B = B_U$ are used as the noise bandwidth for label and payload receivers, respectively, while $R = R_{\text{ph}}$ and $R = R_{\text{pU}}$ are used as the responsivities for label and payload receivers, respectively. $P = P_h$ and $P = P_U$ represent the received average power at label and payload receivers, respectively. The following values are used in both our calculation and experiment: $P_{\text{in}} = -17$ dBm, $G_1 = G_2 = 23$ dB, $L_1 = -13$ dB, $n_{\text{sp}} = 1.6, \Delta v_f = 40$ GHz, $B_U = 7$ GHz.

C. Residual Intensity Noise After a Label Eraser

A perfect label eraser should completely erase the superimposed old label. In the proposed scheme, however, the complementary signal contains undesired random timing error due to the intensity noise to timing jitter conversion at the limiting amplifier shown in Fig. 4. Therefore, we need to characterize the residual noise due to this imperfection. We begin with the E-field after an optical label eraser, which can be written as (10), shown at the bottom of the page, where $H_c(t)$ is the complementary signal of $H(t)$. If $H_c(t)$ is a perfect complementary signal of $H(t)$, then $H(t) + H_c(t) = 1$ and $H(t)H_c(t) = 0$, as shown in Fig. 7, and the net effect of an optical eraser on a payload is simply to multiply the payload E-field by a constant $\sqrt{(1 - m_h)}$. The optical average power and peak power after the label eraser were denoted by P_U and $P_{U,\text{peak}}$, respectively, and can be written as $P_{U,\text{peak}} = (1 - \kappa)P_{\text{peak}}(1 - m)$ and $P_U = P_{U,\text{peak}}(1 - 0.5m_U)$. In reality, however, $H_c(t)$ can be seen as an inverse of $H(t)$ with a relative random jitter $\Delta\tau_i$ on its transition edges. In this case, $H(t) + H_c(t) \neq 1$ and

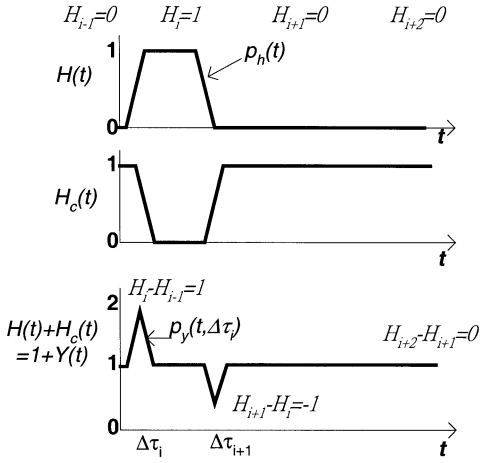

Fig. 7. Illustration of the timing relationship among $H(t)$, $H_c(t)$ and $Y(t)$.

$H(t)H_c(t) \neq 0$, and, consequently, residual noise results. The residual noise due to nonzero $m_h^2 H(t)H_c(t)$ can be neglected when m_h is small, and we will focus our attention on the effect of nonunity $H(t) + H_c(t)$. We note that $H(t) + H_c(t)$ can be decoupled into a dc component and a random pulse chain as

$$\begin{aligned} H(t) + H_c(t) &= 1 + \sum_i Y_i \cdot (p_h(t - iT_h) - p_h(t - iT_h + \Delta\tau_i)) \\ &= 1 + \sum_i Y_i p_y(t - iT_h, \Delta\tau_i) \equiv 1 + Y(t) \end{aligned} \quad (11)$$

where $p_y(t, \Delta\tau_i)$ is the pulse waveform, T_h is the label pulse duration, and the random sequence $Y_i = (H_i - H_{i-1})$ is the difference of adjacent bits of H_i. Fig. 7 illustrates the relationship among $H(t), H_c(t)$ and $Y(t)$. The bit stream of a label is assumed to be random, so the probability function of y_i is $P(Y_i = 1) = P(Y_i = -1) = 0.25$ and $P(Y_i = 0) = 0.5$, and its variance is $\sigma^2_Y = 0.5$. Next, we need to analyze the pulse shape of $p_y(t, \Delta\tau)$ so that the power spectral density of $Y(t)$

$$\begin{aligned} E(t) &= \sqrt{(1 - \kappa)P_{\text{peak}}[((1 - m_U) + m_U U(t))((1 - m_h) + m_h H(t))((1 - m_h) + m_h H_c(t))]}\exp(j\omega_c t + \theta) \\ &= \sqrt{(1 - \kappa)P_{\text{peak}}[((1 - m_U) + m_U U(t))((1 - m_h)^2 + (1 - m_h)m_h(H(t) + H_c(t)) + m_h^2 H(t)H_c(t))]} \\ &\quad \times \exp(j\omega_c t + \theta) \end{aligned} \quad (10)$$

can be calculated. We assume that the label NRZ pulses pass through a Bessel low-pass filter ($\mathrm{LPF_t}$). A Bessel LPF can be approximated as a Gaussian filter; hence, the label pulse can be expressed as [18], [19]

$$p_h(t) = \frac{1}{2}\left[-\mathrm{erfc}\left(\frac{2t}{T}\right) + \mathrm{erfc}\left(\frac{2(t-T_h)}{T}\right)\right] \tag{12}$$

where $\mathrm{erfc}(x) = 2/(\sqrt{\pi})\int_z^\infty \exp(-z^2)dz$ and T is determined by the transmitter filter bandwidth according to $(3/4)TB_{ht} = 0.35$, where B_{ht} is the 3-dB bandwidth of the Bessel $\mathrm{LPF_t}$. If we set $B_{ht} = 80$ MHz, then $T = 5.8$ ns. From Fig. 7, it can be seen that $p_y(t, \Delta\tau)$ results from the difference between two slightly offset leading-edge or trailing-edge pulse waveforms. We can use the difference between two leading-edge waveforms to obtain $p_y(t, \Delta\tau)$ as follows:

$$\begin{aligned} p_y(t,\Delta\tau) &= \left[-\frac{1}{2}\mathrm{erfc}\left(\frac{2t}{T}\right)\right] - \left[-\frac{1}{2}\mathrm{erfc}\left(\frac{2(t-\Delta\tau)}{T}\right)\right] \\ &= \frac{1}{\sqrt{\pi}}\left(\int_{t/(T/2)-\Delta\tau/(T/2)}^{\infty} \exp -(z)^2\, dz \right. \\ &\qquad \left. - \int_{t/(T/2)}^{\infty} \exp -(z)^2 dz\right). \end{aligned} \tag{13}$$

By substituting $t' = t/(T/2)$ into (13), we have

$$\begin{aligned} p_y(t',\Delta\tau) &= \frac{1}{\sqrt{\pi}}\left(\int_{t'-\Delta\tau/(T/2)}^{t'} \exp -(z)^2 dz\right) \\ &= \frac{1}{\sqrt{\pi}}\left(\int_{-\infty}^{\infty} \prod\left(\frac{z-t'}{\Delta\tau/(T/2)}\right)\left(\exp -(z)^2\right)\, dz\right) \\ &= \int_{-\infty}^{\infty} v(t'-z)g(z)dz = v(t') \otimes g(t') \end{aligned} \tag{14}$$

where

$$\prod(t) = \begin{cases} 1, & 0 < t < 1 \\ 0, & \text{otherwise} \end{cases}$$

$$v(t') = \prod\left(-\frac{t'}{\Delta\tau/(T/2)}\right) \tag{15}$$

$$g(t') = \frac{1}{\sqrt{\pi}}(\exp -(t')^2) \tag{16}$$

and $\otimes$ denotes a convolution. Hence, $p_y(t', \Delta\tau)$ is a convolution of a square pulse $v(t')$ and a Gaussian pulse $g(t')$. The Fourier transform of $v(t')$ and $g(t')$ are written as

$$F_v(f) = \frac{\Delta\tau}{T/2}\frac{\sin(\pi f\Delta\tau/(T/2))}{(\pi f\Delta\tau/(T/2))} \tag{17}$$

$$F_g(f) = \exp(-(\pi f)^2) \tag{18}$$

respectively. Hence, the Fourier transform of $p_y(t', \Delta\tau)$ is

$$\begin{aligned} F'_{py}(f) &= F_v(f)F_g(f) \\ &= \frac{\Delta\tau}{T/2}\frac{\sin(\pi f\Delta\tau/(T/2))}{(\pi f\Delta\tau/(T/2))}\exp(-(\pi f)^2) \end{aligned} \tag{19}$$

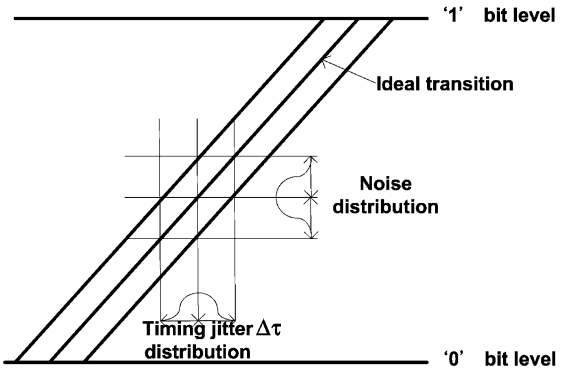

Fig. 8. Illustration on how timing jitter is converted to amplitude noise.

and the Fourier transform of $p_y(t, \Delta\tau)$ can be calculated as

$$\begin{aligned} F_{py}(f) &= \frac{1}{2/T}F'_{py}(\frac{f}{2/T}) \\ &= \Delta\tau\frac{\sin(\pi f\Delta\tau)}{(\pi f\Delta\tau)}\exp(-(\pi fT/2)^2). \end{aligned} \tag{20}$$

Now, $\Delta\tau$ resulted from different pulse edges at different times are different, and we designate them as $\Delta\tau_i, \Delta\tau_{i+1}, \ldots$, etc., as shown in Fig. 7. With a precise length control of the fiber delay line in Fig. 4, the mean of $\Delta\tau_i$ is zero. The variance of $\Delta\tau_i$ can be calculated by assuming that the timing jitter is pattern independent, i.e., $\Delta\tau_i$ are independent random variables.

In generating a complementary signal, the limiting amplifier in Fig. 4 acts as an analog decision circuit and converts intensity noise to phase noise. The standard deviation of the resulting timing jitter $\Delta\tau$ is related to the original signal's intensity noise through the signal waveform's slew rate as follows [20]:

$$\sigma_{\Delta\tau} = \frac{\text{amplitude noise}}{\text{slew rate}} = \frac{A/2Q_c}{0.8A/T_r} = \frac{T_r}{1.6Q_c} \tag{21}$$

as illustrated in Fig. 8. The slew rate in (21) can be approximated by a pulse amplitude divided by a pulse rise time T_r (10–90%) and is given by $0.8A/T_r$, where A is the peak amplitude of the waveform. The root-mean-square (rms) noise amplitude in (21) is related to the signal's Q factor by $\sigma_n = (A/2Q_c)$. We use Q_c to denote the Q factor of the received label. We can clearly see from (21) that a $\mathrm{LPF_r}$ with too narrow a bandwidth introduces a large T_r, and, consequently, the AM-to-PM conversion effect generates unwanted timing jitter. On the other hand, a $\mathrm{LPF_r}$ with too wide a bandwidth includes too much noise and interference. Therefore, there is an optimum bandwidth of $\mathrm{LPF_r}$.

From (21), we can see that $\Delta\tau$ is in sub-nanosecond range when the Q factor is greater than 6 and T_r is in the range of 5–6 ns. Therefore, $\Delta\tau$ is smaller than T, which is fixed at 5.8 ns, as mentioned previously, and we can let $((\sin(\pi f\Delta\tau))/(\pi f\Delta\tau)) = 1$. As a result, (20) can be simplified to become

$$F_{py}(f) \approx \Delta\tau\exp(-(\pi fT/2)^2) \tag{22}$$

by having $((\sin(\pi f\Delta\tau))/(\pi f\Delta\tau)) \approx 1$. The inverse Fourier transform of (22) is

$$p_y(t,\Delta\tau) = \frac{\Delta\tau}{T/2}\frac{1}{\sqrt{\pi}}\left(\exp - \left(\frac{t}{T/2}\right)^2\right). \quad (23)$$

From (23), it can be seen that the timing error $\Delta\tau$ has been converted to residual intensity noise, which has a Gaussian pulse shape.

The amount of residual intensity noise after an nth label eraser could affect both the label and payload signals in the $(n+1)$th and following hops. We can derive this residual intensity noise by beginning with the first hop as follows. From (10) and (11), we can derive the photocurrent of the residual intensity noise by considering only the noise induced from $Y(t)$ as

$$I_n(t) = RP\cdot((1-m_U)+m_U U(t))m_h Y(t) \quad (24)$$

where P and R are the received peak power and responsivity of the receiver, respectively. The term $m_h^2 H(t)H_c(t)$ was neglected. When we consider the amount of the residual noise entering the label receiver, we note that the label receiver only sees the average value of payload signal $U(t)(=0.5)$, as was shown in Section III-A. Therefore the photocurrent of the residual noise is $R_{\rm ph}P_{h,\rm peak}(1-(1/2)m_U)m_h Y(t)$.

In order to calculate the residual intensity noise entering the payload receiver, the noise photocurrent in (24) is dissolved into two components: the first is the multiplication of dc bias $(1-(1/2)m_U)$ and $R_{pU}P_{U,\rm peak}m_h Y(t)$, and the second is the multiplication of high-speed ac digital signal $m_U(U(t)-1/2))$ and $R_{pU}P_{U,\rm peak}m_h Y(t)$. The first component is a low-frequency residual intensity noise, which is within the receiver bandwidth of the payload receiver. The second term can be neglected when the residual intensity noise is much smaller than the payload signal power (as will be evidenced in Figs. 15 and 17).

At each hop, this residual noise is added to the optical signal so the residual noise is accumulated along the optical path. From (21), (23), and the definition of $Y(t)$ in (11), the accumulated residual noise from hop 1 to k $-$ 1 seen at the label receiver in the kth hop is

$$\sigma^2_{\rm res,(k)} = \sum_{j=1}^{k-1}(R_{\rm ph}P_{h,\rm peak}(1-(1/2)m_U)m_h)^2\sigma^2_{\Delta\tau,(j)} \times \sigma^2_{\rm Y}(1/T_h)\int_{-\infty}^{\infty}|F_{\rm rh}(f)|^2\left|\exp(-(\pi fT/2)^2)\right|^2 df \quad (25)$$

where $\sigma^2_{\Delta\tau,(j)}$ is the timing jitter variance of the complementary signal at the jth hop. Note that $\sigma^2_{\rm res,(k)} = 0$ for k < 2.

The payload receiver filter bandwidth is much wider than the residual noise, so the total residual noise seen by the payload receiver at the kth hop is given by

$$\sigma^2_{\rm res,(k)} = \sum_{j=1}^{k-1}(R_{pU}P_{U,\rm peak}(1-(1/2)m_U)m_h)^2\sigma^2_{\Delta\tau,(j)} \times \sigma^2_{Y}(1/T_h)\int_{-\infty}^{\infty}\left|\exp(-(\pi fT/2)^2)\right|^2 df. \quad (26)$$

We will see later that the total distance and the number of hops in a multihop link are mainly limited by the label signal degradation rather than by the payload signal degradation.

D. Receiver Noise

The receiver noise includes thermal and shot noise. The total power of receiver thermal noise is given by $\sigma^2_{\rm th} = ((4KT_a)/(R_e))F_eB$ and that of shot noise is given by $\sigma^2_{\rm sh} = 2qRPB$. Note that $B = B_{\rm hr}$ and $B = B_U$ are used as the noise bandwidth for the label and payload receiver, respectively, while $R = R_{\rm ph}$ and $R = R_{pU}$ are the responsivities for label and payload receivers, respectively. $P = P_h$ and $P = P_U$ are used as the receiver average power to the label and payload receivers, respectively. The following values are used in both our calculation and experiment: responsivity $R_{pU} = R_{\rm ph} = 0.9$, load resistance $R_e = 50\ \Omega$, receiver noise figure $F_e = 2$ dB, and $T_a = 300\ ^\circ$K.

E. Overall Q-Factor Performance of a Label

The system performance is related less to the received raw label signal than to the complementary signal, which is a reshaped version of the old label signal. Therefore, we are more concerned about how to obtain a low-jitter complementary signal. As will become clear in Section V-B, the required received optical power to obtain a low jitter complementary signal, defined as P_h^c, is several decibels higher than the label receiver sensitivity P_h (see Section V-B). When the average received power is P_h, the unfiltered label signals at mark and space are given by (see Section III-A)

$$I_{h,1} = R_{\rm ph}\frac{P_h}{(1-0.5m_U)(1-0.5m_h)}[(1-m_U)+m_U(1/2)]$$
$$I_{h,0} = R_{\rm ph}\frac{P_h}{(1-0.5m_U)(1-0.5m_h)}[(1-m_U)(1-m_h) + (1-m_h)m_U(1/2)] \quad (27)$$

and the total noise variance is the combination of all noise terms obtained in Section III, as follows:

$$\sigma^2_{h1,(k)} = \sigma^2_{\rm spsp,(k)} + \sigma^2_{\rm sig-sp,(k)} + \sigma^2_{\rm th} + \sigma^2_{\rm sh} + \sigma^2_{\rm it,1} + \sigma^2_{\rm res,(k)}$$
$$\sigma^2_{h0,(k)} = \sigma^2_{\rm spsp,(k)} + \sigma^2_{\rm sig-sp,(k)} + \sigma^2_{\rm th} + \sigma^2_{\rm sh} + \sigma^2_{\rm it,0} + \sigma^2_{\rm res,(k)}. \quad (28)$$

Therefore, we obtain the Q factor of the label at the kth hop as

$$Q_h = \frac{(I_{h,1}-I_{h,0})\gamma}{\sigma_{h0,(k)}+\sigma_{h1,(k)}} \quad (29)$$

where γ is the eye-closure percentage caused by the receiver filter bandwidth. As a reminder, $P^c_{\rm avg}$ was used in (27)–(29) to obtain the Q_c in (21) and the corresponding residual noise at the kth hop for $k > 1$.

F. Overall Q-Factor Performance of a Payload

The amplitudes of the received payload at mark and space are respectively given by

$$I_{U,1} = R_{pU}\frac{P_U}{(1-0.5m_U)}$$
$$I_{U,0} = R_{pU}\frac{P_U(1-m_U)}{(1-0.5m_U)} \quad (30)$$

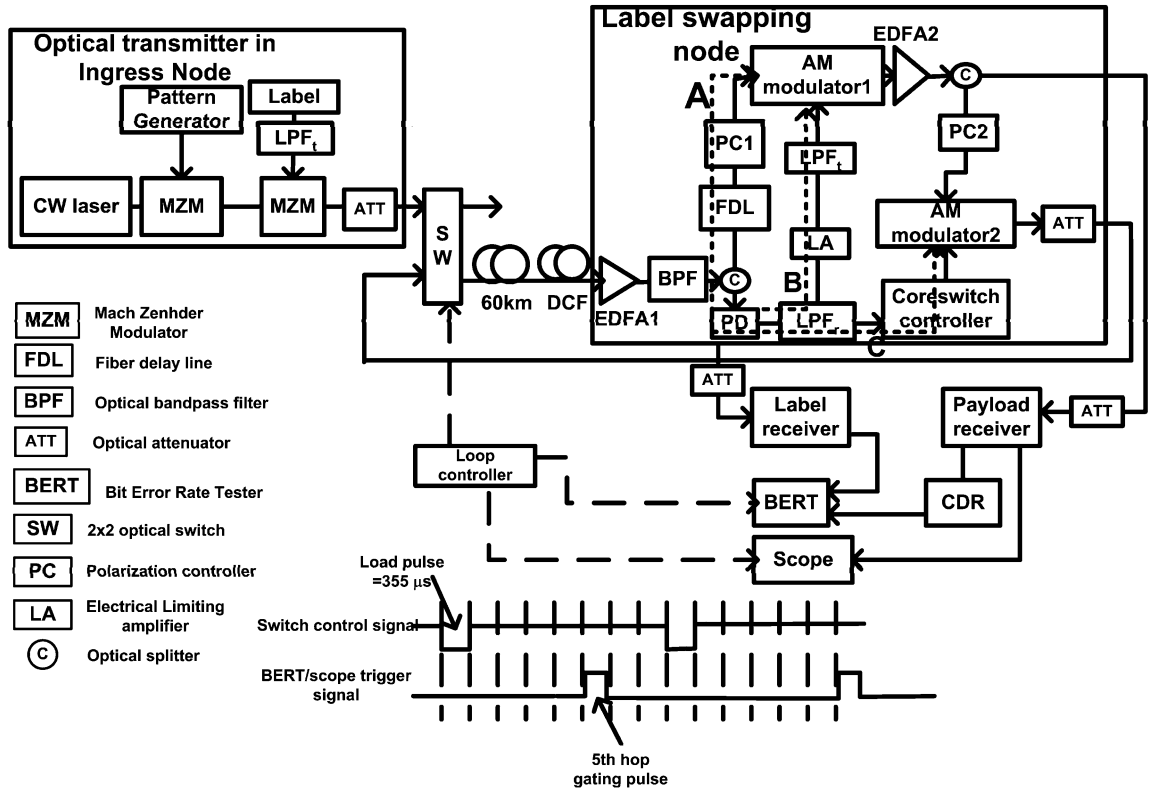

Fig. 9. Experimental setup.

where P_U is the average received power, and the noise power of mark and space are

$$\sigma^2_{U1,(k)} = \sigma^2_{\mathrm{spsp},(k)} + \sigma^2_{\mathrm{sig-sp},(k)} + \sigma^2_{\mathrm{th}} + \sigma^2_{\mathrm{sh}} + \sigma^2_{\mathrm{res},(k)}$$
$$\sigma^2_{U0,(k)} = \sigma^2_{\mathrm{spsp},(k)} + \sigma^2_{\mathrm{th}} + \sigma^2_{\mathrm{res},(k)}. \quad (31)$$

Finally, at the kth hop, the payload Q factor is given by

$$Q_U = \frac{I_{U,1} - I_{U,0}}{\sigma_{U0,(k)} + \sigma_{U0,(k)}}. \quad (32)$$

IV. Experimental Setup

The experimental setup of a recirculating loop, shown in Fig. 9, was built to test the feasibility and scalability of the proposed optical-label-swapping scheme. It can be seen that there was an optical transmitter, a payload receiver, a label receiver, and a 60-km recirculating loop. The loop by itself consists of 60-km single-mode fiber, a dispersion-compensating fiber (DCF) module which provides a total compensation of −988 ps/nm, two EDFAs, and the label-swapping apparatus. The input power to the 60-km fiber is kept below 0 dBm to minimize fiber nonlinear effects. A 50-GHz optical bandpass filter was used to remove out-of-band ASE noise. The input power to EDFA1 and EDFA2 were −17 dBm and −7 dBm, respectively. An optical attenuator was used to carefully balance the gain and loss of the loop. The total loop propagation delay was 355 μs. A loop controller was programmed to provide gating signals to a 2×2 optical switch, a BER tester, and a sampling scope. The payload and label signal performance can thus be measured at any hop after any number of recirculations.

The optical transmitter was composed of a CW laser and two $LiNbO_3$ external modulators. The first modulator was driven by an 8B/10B-coded 10 Gb/s with a PRBS length of $2^{31} - 1$ (again, the payload's raw data pattern length is not very important because the 8B/10B encoder will limit the maximum of run length to 5). The extinction ratio of the modulator is set to be 10 dB. The second modulator was driven by a 100-Mb/s NRZ label signal with a PRBS length of $2^7 - 1$ and modulation depth $m_h = 0.2$. Note that before the label signal was sent to the modulator, there was a Bessel pulse -shaping filter $(\mathrm{LPF_t})$ with a bandwidth B_{ht} of 80 MHz. Fig. 10 shows the eye diagram of a transmitted 8B/10B-coded 10-Gb/s payload which has a superimposed 100-Mb/s ASK label. Fig. 11 shows the measured power spectra of the transmitted 100- Mb/s NRZ label, 8B/10B-coded 10-Gb/s payload, and their combination. Note in particular that the 8B/10B line code provides a low interference power to the label at low-frequency range.

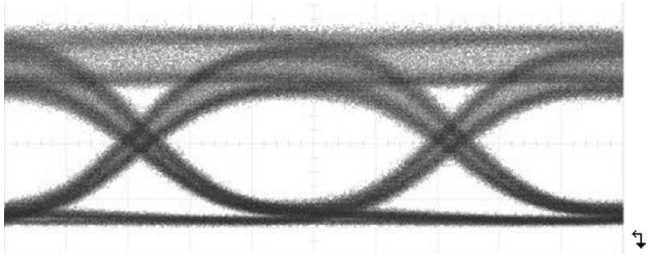

Fig. 10. Measured eye diagram of a transmitted 8B/10B-coded 10-Gb/s payload that has a superimposed 100-Mb/s ASK label.

At the input port of the recirculating loop, an optical splitter was used to tap a portion of the optical power for receiving the old label. The label receiver had a fifth-order front-end Bessel filter $(\mathrm{LPF_r})$ with a 60-MHz bandwidth to remove most of

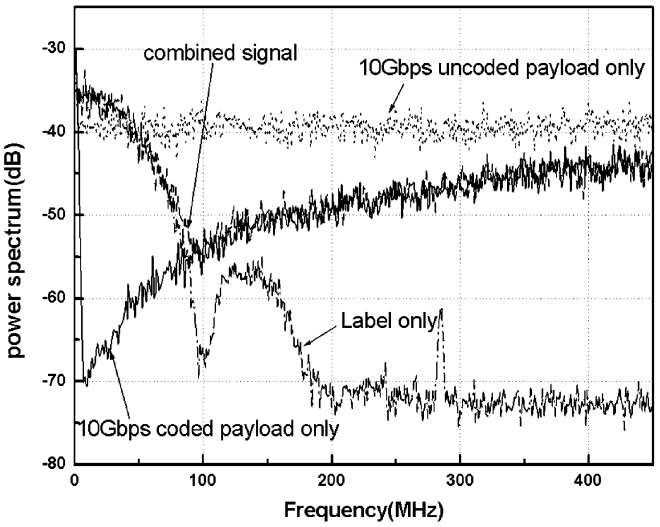

Fig. 11. Power spectra of a transmitted 100-Mb/s NRZ label, an 8B/10B-coded 10-Gb/s payload, and their combination.

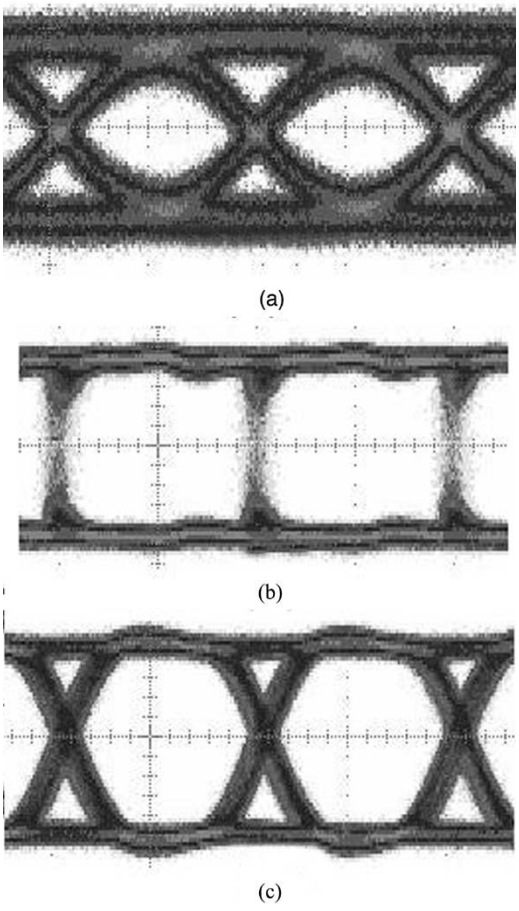

Fig. 12. Eye diagrams of the received label: (a) after a 60-MHz frond-end Bessel $\mathrm{LPF_r}$; (b) after a limiting amplifier; and (c) after a second pulse shaping $\mathrm{LPF_t}$ whose bandwidth is exactly the same as that in the transmitter end.

the payload interference, a limiting amplifier, and an additional fifth-order low-pass Bessel filter $(\mathrm{LPF_t})$ to further amplify and reshape the received waveform, respectively, so that the complementary signal can be obtained. Fig. 12 shows the eye diagrams after each of the three stages. Optimum filter bandwidth will be discussed in the next section. The complementary signal was subsequently used to modulate the incoming composite signal of the payload and old label through an external modulator with an inverse logic. The old label was then erased, but with some remaining residual noise, as was analyzed previously. Note that in order to erase the old label as much as possible, three conditions need to be satisfied.

1) The optical fiber delay line in Fig. 9 should be adjusted so that the propagation delays between the paths A and B (marked by the thick dotted lines in Fig. 9) are equal.
2) The modulation depth of the complementary signal should be adjusted to be the same as that in the transmitter.
3) $\mathrm{LPF_t}$ in the complementary signal generation path should be the same as that in the transmitter.

A new label was generated from a switch controller and combined with the "cleaned" payload through path C in Fig. 9, where a second AM modulator was used. All modulators had a 3-dB bandwidth of 20 GHz and an insertion loss of 5 dB in normal operation. All modulators had input polarization controllers to maintain modulation efficiency and loop power balance.

For each circulation of the composite signal, BER performances of both the payload and label can be measured, as shown in Fig. 9. Note that the payload should be coupled out of the loop after the output of the first AM modulator where the old label has been erased. A payload receiver consists of a p-i-n photoreceiver and a clock and data recovery (CDR) circuit. Due to the existence of transient discontinuity between successive circulated signals, the CDR needed $\sim 5\ \mu$s to extract the clock and recover the payload data. In the experimental setup, the BER tester and oscilloscope were both triggered by the loop controller in Fig. 9. The label signal was sent to a field-programmable gate-array (FPGA)-based switch controller for CDR, and its BER performance was analyzed by a BER tester.

V. Results and Discussion

In this section, the analytical and experimental results are compared. Design guidelines on how to optimize the front-end filter bandwidth in a label receiver and on how to minimize the accumulated residual noise from multiple optical label erasers in a multihop system are presented.

A. Optimum Bandwidth of the Low-Pass Filter $\mathrm{LPF_r}$

As we saw in Section III, the frond-end bandwidth of a label receiver $(\mathrm{LPF_r})$ is an important parameter to the performance of a label signal. A wide filter bandwidth means more interference noise (from payload) and thermal noise could be included, whereas a narrow filter bandwidth implies not only worsened signal waveform distortion but also more timing jitter in the complementary signal, as can be seen in (21). The residual intensity noise converted by a complementary signal's undesired jitter via a limiting amplifier could be accumulated through multiple hops, while the interference and thermal noise are not accumulated through multiple hops. Consequently, the optimum $\mathrm{LPF_r}$ bandwidth depends on which noise term is dominant. For

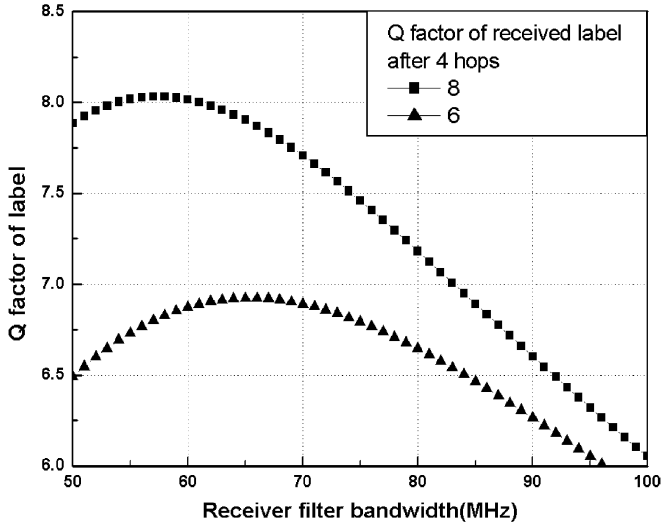

Fig. 13. Numerical calculation of the Q factor of the label at the fifth hop versus various receiver front-end LPF bandwidths, under several Q factors of the received label after 4 hops (considering only $\sigma_{\rm it}$ and $\sigma_{\rm res}$). $m_U = 0.9, m_h = 0.2$.

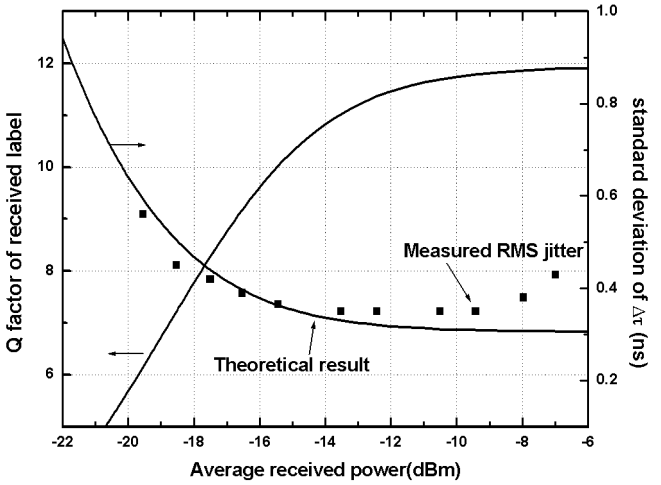

Fig. 14. Received label waveform quality and timing jitter performance of a complementary signal versus $P_h^c, m_U = 0.9, m_h = 0.2$ (dots were measured after the first hop).

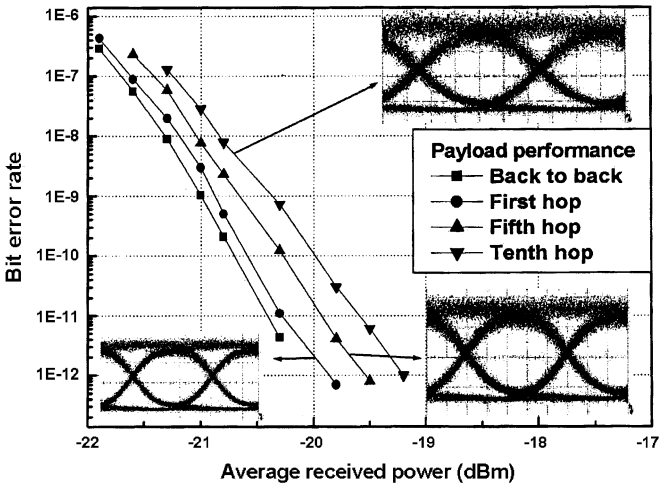

Fig. 15. Measured 8B/10B-coded 10-Gb/s payload BER performance in a multihop experiment. $m_U = 0.9, m_h = 0.22, P_h^c = -14$ dBm.

example, if the received label has a high Q factor, the accumulated residual noise may be smaller than the interference and thermal noise. In this case, the filter bandwidth should be decreased to cut off the interference and thermal noise. On the other hand, if the received label has a low Q factor, meaning that the accumulated residual intensity noise is already high, the filter bandwidth should be wider to avoid causing more jitter noise. Fig. 13 illustrates these two examples by letting Q_c equal to 8 and 6 after 4 hops. We can see that the optimum filter bandwidth is 58 and 68 MHz, respectively.

Since we are more interested in knowing the maximum transmission distance through multiple hops, we need to prevent rapid accumulation of residual intensity noise, so the received optical power into a label receiver needs be increased to obtain a higher Q factor for the received label. Consequently, we used a fifth-order Bessel filter with a 60-MHz bandwidth in our experiment. It is noted that this narrow filter bandwidth only induces little eye-closure penalty—the eye-closure penalty γ used in (29) is equivalent to 0.98, according to our measurement.

B. Dynamic Range of a Label Eraser

We learned from the previous section and (21) that we wish to receive a higher optical power into the label receiver to reduce the undesired timing jitter of the complementary signal, so that the residual intensity noise from a nonideal label eraser can be minimized over multiple hops. To achieve this target, one can place the label receiver after EDFA1 to increase the received optical power. We carried out an experiment to confirm this conjecture, as shown in Fig. 14 (obtained at the first hop). In the figure, we show the Q factor of a received label and the resulting rms jitter on the complementary signal as a function of the received optical power into a label receiver. We can see a significant improvement in both parameters when the received optical power is increased beyond approximately -14 dBm, e.g., the timing jitter of 600 ps at a received power of -19.5 dBm can be reduced to 360 ps at -14 dBm. Measured results agree well with what is predicted from (21). The deviation at a received optical power higher than -14 dBm is due to the limited dynamic range of the receiver transimpedance amplifier. In our experiment, the optical label eraser provides a consistent good performance from -14 to -8 dBm. Note that in this scheme, the 100-Mb/s label receiver sensitivity is much worse than a conventional 100-Mb/s digital receiver. This is because the modulation index m_h was controlled to be small enough to minimize the impact on the payload signal and because the presence of the payload signal generates significant interference noise on the label signal.

C. Multihop Payload and Label Performance

Figs. 15 and 16 show the multihop BER performances of the 8B/10B-coded 10-Gb/s payload and the 100-Mb/s ASK optical label, respectively. We can see that after 10 hops and a total transmission distance of 600 km, the payload receiver power penalty at a BER of 1×10^{-9} is less than 0.8 dB. The eye diagrams of the 10-Gb/s payload after 1, 5, and 10 hops are shown in the insets of Fig. 15. No obvious signal degradation can be

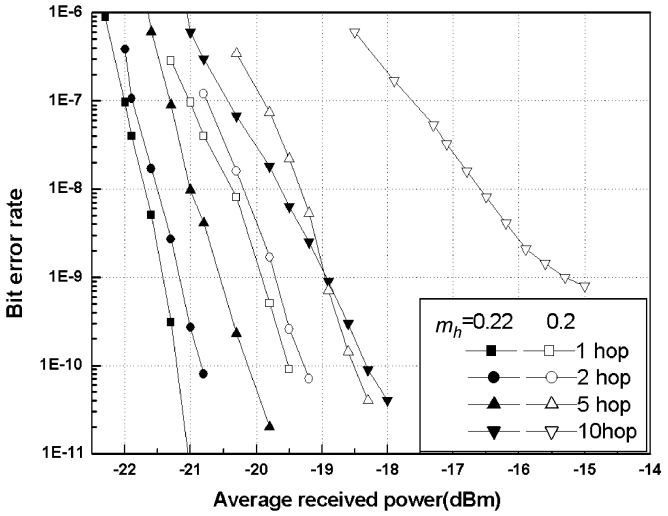

Fig. 16. Measured 100-Mb/s ASK label performance in a multihop recirculating loop experiment. $m_U = 0.9, P_h^c = -14$ dBm.

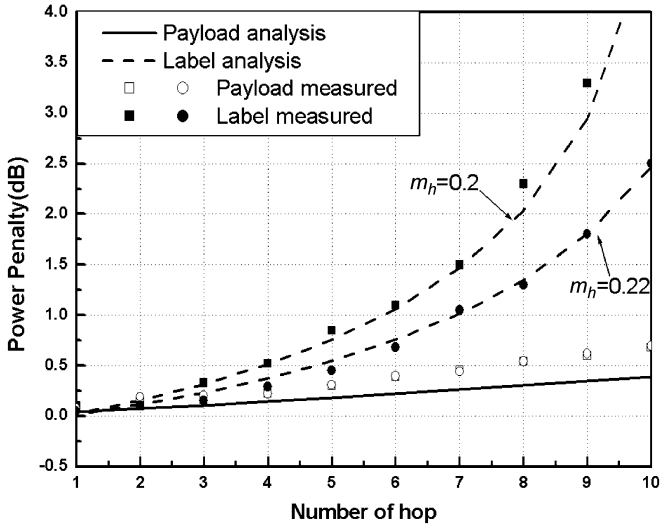

Fig. 17. Power penalties at different numbers of hops, $m_U = 0.9, P_h^c = -14$ dBm. Line: Theory. Dot: Experimental results.

observed. The label BER performances after different numbers of hops and at modulation depths of 0.2 and 0.22 are shown in Fig. 16. We can see that after 10 hops and 600 km, the system power penalties are 4.5 and 2.5 dB at $m_h = 0.2$ and 0.22, respectively. Note that an error floor occurs around a BER of 1×10^{-9} when $m_h = 0.2$. The reason why a 10% increase of m_h can make a big difference in the ASK label performance is because the accumulated residual noise grows very rapidly (instead of linearly proportional to the number of hops) once a complementary signal begins to have a timing jitter above a certain threshold level. This is because the label quality at the nth hop is always worse than that at the $(n-1)$th hop under a fixed received optical power for every hop. Note that the label's signal quality drops quickly after 10 hops, even when $m_h = 0.22$. In this experiment, the label receiver input power is chosen at -14 dBm.

Fig. 17 shows the power penalties versus the number of hops for payload and label at a BER of 1×10^{-9}. The Q factor of label and payload at different hops are obtained from (29) and (32). By assuming that the combined noise is a Gaussian noise, we can calculate the BERs from$Q$ factors and the power penalties at 1×10^{-9}, and the results are given in Fig. 17. The analytical results match well with the experimental results for the label and payload signals, respectively.

The requirement on the number of hops depends on the network environment. Typically, most of the hop counts between two end nodes in a 100-node mesh network range from four to ten [21]. Our experimental demonstration shows that the new optical-label-swapping scheme can be comfortably applied to this typical multihop network environment. As a matter of fact, the total number of hops and the transmission distance demonstrated set an experimental record among all reported optical-label-swapping schemes.

If the number of hops required in a high-speed core network is more than ten, we can possibly use an all-optical reshaper to further clean the residual noise. However, we must point out that most all-optical reshapers have small dynamic range [22] and may complicate practical network designs.

VI. Conclusion

We have successfully demonstrated a novel all-optical-label-swapping scheme by superimposing a 100-Mb/s ASK label signal on top of an 8B/10B-coded 10-Gb/s payload. The superimposed optical label requires only 25% extra transmission bandwidth and can be optically erased by modulating the composite signal of payload and label with the inverse of the received optical label signal. By carefully designing the label receiver front end and reshaping filters, and by maintaining the optical power to a label receiver beyond -14 dBm, we have been able to minimize the unavoidable timing jitter during the label erasure process. As a result, we have been able to obtain satisfactory experimental results after 10 hops of optical label swapping and 600-km transmission by using a recirculating loop. This transmission performance can be further improved, provided 1) building integrated timing supply (BITS) clock and digital CDR circuits with a high oversampling rate (to reduce the delay variations from packet to packet) can be implemented inside the label eraser and 2) a line code with a better dc-balanced characteristics and a higher coding efficiency than 8B/10B can be found.

We have also developed a complete analysis to explain the system limitation due to the accumulated residual timing jitter in multiple label erasure processes. We have also provided clear guidelines on how to optimize the modulation depths of both payload and label and how to optimize the bandwidth of a label receiver front-end low-pass filter. We note that the superimposed ASK label also suffers low extinction ratio due to the presence of some residual payload in the low-frequency range. This can be compared with the low extinction ratio suffered by high-speed payload signals in orthogonal modulation techniques [6]–[8]. Since the label signal is swapped in every switching node while the high-speed payload cannot be, the superimposed ASK labeling technique can supposedly go through a longer transmission distance. In conclusion,

we believe that the novel and simple optical-label-swapping scheme can be applied to the next-generation core networks.

REFERENCES

[1] A. Banerjee *et al.*, "Generalized multiprotocol label switching: An overview of routing and management enhancements," *IEEE Commun. Mag.*, pp. 144–150, Jan. 2001.

[2] C. Gullemon *et al.*, "Transparent optical packet switching: The European ACTS KEOPS project approach," *J. Lightwave Technol.*, vol. 16, pp. 2117–2134, Dec. 1998.

[3] J. Cao, M. Jeon, Z. Pan, Y. Bansal, Z. Wang, Z. Zhu, V. Hernandez, J. Taylor, V. Akella, S. Yoo, K. Okamoto, and S. Kamei, "Error-free multi-hop cascaded operation of optical label switching routers with all-optical label swapping," in *OFC 2003*, vol. 2, Atlanta, GA, Mar. 2003, pp. 791–792.

[4] G. Rossi, O. Jerphagnon, B.-K. Olsson, and D. Blumenthal, "Optical SCM data extraction using a fiber-loop mirror for WDM network systems," *IEEE Photon. Technol. Lett.*, vol. 12, pp. 897–899, July 2000.

[5] Y. M. Lin, W. I. Way, and G. K. Chang, "A novel optical label swapping technique using erasable optical single-sideband subcarrier label," *IEEE Photon. Technol. Lett.*, vol. 12, pp. 1088–1091, Aug. 2000.

[6] N. Chi, J. Zhang, P. V. Holm-Nielsen, L. Xu, I. T. Monroy, C. Peucheret, K. Yuind, L. J. Christiansen, and P. Jeppesen, "Experimental demonstration of cascaded transmission and all-optical label swapping of orthogonal IM/FSK labeled signal," *Electron. Lett.*, vol. 39, pp. 676–679, Apr. 2003.

[7] N. Chi, J. Zhang, P. V. Holm-Nielsen, C. Peucheret, and P. Jeppesen, "Transmission and transparent wavelength conversion of an optically label signal using ASK/DPSK orthogonal modulation," *IEEE Photon. Technol. Lett.*, vol. 15, pp. 760–762, May 2003.

[8] M. Ohm and J. Speidel, "Quaternary optical ASK-DPSK and receivers with direct detection," *IEEE Photon. Technol. Lett.*, vol. 15, pp. 159–161, Jan. 2003.

[9] F. Liu, C. J. Rasmussen, and R. J. S. Pedersen, "Experimental verification of a new model describing the influence of incomplete signal extinction ratio on the sensitivity degradation due to multiplex interferometric crosstalk," *IEEE Photon. Technol. Lett.*, vol. 11, pp. 137–139, Jan. 1999.

[10] *Fiber Channel-Physical and Signaling Interface*, ANSI Standard X3.230, 1994.

[11] J. G. Proakis, *Digital Communications*, 3rd int. ed. New York: McGraw-Hill, 1995, pp. 203–223.

[12] D. Wolfson, S. L. Danielsen, H. N. Poulsen, P. B. Hansen, and K. E. Stubkjaer, "Experimental and theoretical investigation of the regenerative capacilities of electrooptic and all-optical interferometric wavelength converters," *IEEE Photon. Technol. Lett.*, vol. 10, pp. 1413–1415, Oct. 1998.

[13] M. C. Yuang, J. Shih, and P. L. Tien, "Traffic shaping for IP-over-WDM networks based on optical coarse packet switching paradigm," in *Proc. ECOC-IOOC 2003*, Rimini, Italy, Sept. 2003, We4, p. 148.

[14] ——, "QoS burstification of optical burst switched WDM networks," in *Proc. OFC'02*, pp. 781–783. ThGG118.

[15] M. C. Chia, D. K. Hunter, I. Andonovic, P. Ball, I. Wright, S. P. Ferguson, K. M. Guild, and M. J. O'Mahony, "Packet loss and delay performance of feedback and fee-forward arrayed-waveguide gratings-based optical packet switches with WDM input-outputs," *J. Lightwave Technol.*, vol. 19, pp. 1241–1254, Sept. 2001.

[16] N. A. Olsson, "Lightwave systems with optical amplifiers," *J. Lightwave Technol.*, vol. 7, pp. 1071–1082, July 1989.

[17] K. Iizuka, *Elements of Photonics: Vol. II for Fiber and Integrated Optics*. New York: Wiley, 2002.

[18] M. C. Jeruchim, P. Balaban, and K. S. Shanmugan, *Simulation of Communication Systems*, 2nd ed. Norwell, MA: Kluwer, p. 140.

[19] VPIsystem Inc. VPItransmissionMaker V4.5. [Online] Available: http://www.vpisystems.com

[20] M. Shimanouchi, "An approach to consistent jitter modeling for various jitter aspects and measurement methods," in *Int. Test Conf. 2001*, Oct. 2001, pp. 848–857.

[21] H. Wessing, H. Christiansen, T. Fjelde, and L. Dittmann, "Novel scheme for packet forwarding without header modifications in optical networks," *J. Lightwave Technol.*, vol. 20, pp. 1277–1283, Aug. 2002.

[22] S. L. Danielsen, P. B. Hansen, K. E. Stubkjaer, M. Schilling, K. Wunstel, W. Idler, P. Doussiere, and F. Pommerau, "All optical wavelength conversion schemes for increased input power dynamic range," *IEEE Photon. Technol. Lett.*, vol. 10, pp. 60–62, Jan. 1998.

Yu-Min Lin received the B.S. degree in electrical engineering from National Tsing-Hua University, Taiwan, R.O.C., in 1996 and the Ph.D. degree in communication engineering from National Chiao-Tung University, Hsinchu, Taiwan, R.O.C., in 2003.

He joined the Department of Optical Communications and Networks, Industrial Technology Research Institute (ITRI), Taiwan, R.O.C., in 2004. His research interests include broad-band optical networking and optical packet switching.

Maria C. Yuang received the B.S. degree in applied mathematics from the National Chiao-Tung University, Hsinchu, Taiwan, R.O.C., in 1978, the M.S. degree in computer science from the University of Maryland, College Park, in 1981, and the Ph.D. degree in electrical engineering and computer science from the Polytechnic University, Brooklyn, NY, in 1989.

She was with AT&T Bell Laboratories and Bell Communications Research (Bellcore) from 1981 to 1990, where she was a Member of Technical Staff working on high-speed networking and protocol engineering. She was also an Adjunct Professor at the Department of Electrical Engineering, Polytechnic University, from 1989 to 1990. In 1990, she joined National Chiao-Tung University, where she is currently a Professor of the Department of Computer Science and Information Engineering. Her current research interests include optical and broad-band networking, multimedia communications, wireless local/access networking, and performance modeling and analysis.

San-Liang Lee (S'92–M'95) received the B.S. degree in electronics engineering from National Chiao-Tung University, Hsinchu, Taiwan, R.O.C., in 1984, the M.S. degree in electrical engineering from National Taiwan University, Taipei, Taiwan, R.O.C., in 1986, and the Ph.D. degree in electrical and computer engineering from the University of California, Santa Barbara (UCSB), in 1995.

He joined the faculty of the Department of Electronic Engineering, National Taiwan University of Science and Technology (NTUST), Taipei, Taiwan, R.O.C., in 1988. He became an Associate Professor in 1995 and a Professor in 2002. He is currently Director of the Center for Optoelectronic Science and Technology, School of Electrical and Computer Engineering, NTUST. His research interests include optoelectronic components, photonic integrated circuits, and optical switching technologies. He has published more than 50 referred papers in international journals and conferences.

Dr. Lee is a Member of the IEEE Lasers & Electro-Optics Society (LEOS) and the IEEE Communications Society.

Winston I. Way (S'82–M'82–SM'88–F'01) received the M.S. and Ph.D. degrees from the University of Pennsylvania, Philadelphia, in 1981 and 1983, respectively.

He was with Applied Research, Bellcore (now Telcordia), Red Bank, NJ, from 1984 to 1992, where he pioneered research in subcarrier-multiplexed lightwave systems and conducted a number of well-known dense-wavelength-division-multiplexing (DWDM) digital/analog video transmission experiments. From 1992 to 2000, he was a Professor at the National Chiao-Tung University, Hsinchu, Taiwan, R.O.C., where he continued leading many research projects in HFC systems and networks. From 1998 to 2000, he was also a Consultant at Telcordia, conducting research on next-generation Internet optical networks. In 2000, he founded OpVista Inc., Irvine, CA, and has been developing ultra-DWDM transmission equipment. He is the author of the book *Broadband Hybrid/Fiber Coax System Technologies* (Academic, 1998), has published more than 100 journal and conference papers, and holds more than a dozen published or pending U.S. patents.

Dr. Way has served on the technical program committees of OFC, MTT, OECC, the IEEE Lasers & Electro-Optics Society (LEOS) in (OSA).